# Supplementary Information

*Redox Dynamics of Glutathione in the Intermembrane Space of Mitochondria Impact the Mia40 Redox State*

**Kerstin Kojer[1], Melanie Bien[1], Heike Gangel[1], Bruce Morgan[2], Tobias P. Dick[2] and Jan Riemer[1]**

[1] Cellular Biochemistry, University of Kaiserslautern, Erwin-Schrödinger-Str. 13, 67663 Kaiserslautern, Germany

[2] Division of Redox Regulation, DKFZ-ZMBH Alliance, German Cancer Research Center (DKFZ), Im Neuenheimer Feld 280, 69120 Heidelberg, Germany

**Address correspondence to:** Jan Riemer, Cellular Biochemistry, University of Kaiserslautern, Erwin-Schrödinger-Str. 13/441, 67663 Kaiserslautern, Germany, Phone: +49-631-2052885, Email: jan.riemer@biologie.uni-kl.de

**3** supplementary tables

**9** supplementary figures

# Table S1. $E_{GSH}$ values

| Strains[a] | Carbon Source and Chemical Treatment | $E_{GSH}$ [mV][b] | | | Reference |
|---|---|---|---|---|---|
| | | Cytosol | IMS | Matrix | |
| **Sensor: Grx1-roGFP2, monitored by fluorescence spectroscopy** | | | | | |
| wt | Galactose | -306 ± 1.3 | -301 ± 5 | -301 ± 2 | this study Fig. 1 + 2 |
| Δ*glr1* | Galactose | -284 ± 3.8 | -278 ± 3.4 | -263 ± 2.5 | this study Fig. 3 |
| Δ*glr1* + *GLR1* | Galactose | -302 ± 1.5 | -296 ± 3 | -294 ± 2.5 | this study Fig. 3 |
| Δ*glr1* + cyto-*GLR1* | Galactose | -303 ± 5.5 | -293 ± 1 | -269 ± 2.7 | this study Fig. 3 |
| Δ*zwf1* | Galactose | -292 ± 2.4 | -295 ± 0.9 | -297 ± 3.6 | this study Fig. 3 |
| wt + 10 µM Antimycin A | Galactose; 30'/ 30°C | -309 ± 1.2 | -305 ± 2.7 | 297 ± 2.8 | this study Fig. 5 |
| wt + 1 mM KCN | Galactose; 1 h/ 30°C | -307 ± 2.4 | -312 ± 7.4 | -300 ± 1.7 | this study Fig. 5 |
| wt + 5 mM Paraquat | Galactose; 30'/ 30°C | -306 ± 0.6 | -302 ± 4.1 | -286 ± 1.5 | this study Fig. 5 |
| wt | Glycerol | -304 ± 2.6 | -298 ± 2.7 | -289 ± 3.8 | this study Fig. 5 |
| wt + 2 µM Antimycin A | Glycerol; 30'/ 30°C | -304 ± 1.7 | -298 ± 6.2 | -297 ± 2.6 | this study Fig. 5 |
| wt + 1 mM KCN | Glycerol; 1 h/ 30°C | -308 ± 3.4 | -307 ± 3.5 | -296 ± 3.9 | this study Fig. 5 |
| wt + 5 mM Paraquat | Glycerol; 30'/ 30°C | -306 ± 1 | -302 ± 1.8 | -289 ± 4 | this study Fig. 5 |
| Δ*nde1* | Galactose | -308 ± 2.6 | -311 ± 8.8 | -297 ± 3.8 | this study Fig. 5 |
| Δ*nde2* | Galactose | -308 ± 4.3 | -314 ± 5.8 | -300 ± 1.9 | this study Fig. 5 |
| Δ*rip1* | Galactose | -306 ± 2.2 | -304 ± 3.2 | -298 ± 2.5 | this study Fig. 5 |
| Δ*cox17* | Galactose | -306 ± 0.9 | -305 ± 4.8 | -297 ± 2.8 | this study Fig. 5 |
| Δ*ccp1* | Galactose | -309 ± 1 | -308 ± 2.6 | -301 ± 0.7 | this study Fig. 5 |
| Δ*sod1* | Galactose | -308 ± 0.9 | -299 ± 3.5 | -294 ± 1 | this study Fig. 5 |
| Δ*sod2* | Galactose | -308 ± 1.3 | -301 ± 7.1 | -298 ± 1.2 | this study Fig. 5 |
| Gal10-Mia40 upregulated | 24 h in Galactose | -308 ± 3.3 | -305 ± 12.3 | -303 ± 7.2 | this study Fig. 5 |
| GalL-Erv1 upregulated | 24 h in Galactose | -301 ± 2.8 | -289 ± 3 | -296 ± 2.8 | this study Fig. 5 |
| Δ*por1* | Galactose | -308 ± 1.9 | -271 ± 9.2 | -296 ± 1.2 | this study Fig. 6 |
| wt | Glucose | -310 | - | - | Morgan et al, 2011 |
| Δ*glr1* | Glucose | -290 | - | - | Morgan et al, 2011 |
| HeLa cells (*H. sapiens*) | Glucose | -320 | - | - | Gutscher et al, 2008 |
| **Sensor: roGFP1 / roGFP2, monitored by fluorescence spectroscopy** | | | | | |
| HeLa cells (*H. sapiens*)[c] | Glucose | - | - | -298 | Hanson et al, 2004 |
| wt (*P. pastoris*)[c] | Glucose | -295 | - | - | Delic et al, 2010 |
| wt (*A. thaliana*)[d] | - | -315 | - | - | Meyer & Dick, 2010 |
| **Sensor: rxYFP, monitored by fluorescence spectroscopy** | | | | | |
| wt | Glucose | -289 | - | - | Ostergaard et al, 2004 |
| wt (*E. coli*) | Glucose | -259 | - | - | Ostergaard et al, 2001 |
| Δ*trxB*[e] (*E. coli*) | Glucose | -237 | - | - | Ostergaard et al, 2001 |
| **Sensor: rxYFP, monitored by redox Western Blot** | | | | | |
| wt | Glucose | -286 ± 5 | -255 ± 3 | -296 ± 5[f] | Hu et al, 2008 |
| Δ*glr1* | Glucose | -252 ± 2 | -259 ± 6 | -267 ± 3[f] | Hu et al, 2008 |
| wt | Glucose | -297 | - | - | Dardalhon et al, 2012 |
| Δ*glr1* | Glucose | -261 | - | - | Dardalhon et al, 2012 |
| Δ*trr1*[g] | Glucose | -277 | - | - | Dardalhon et al, 2012 |
| Δ*trx1* Δ*trx2*[h] | Glucose | -277 | - | - | Dardalhon et al, 2012 |
| Δ*trr1* Δ*trx1* Δ*trx2* | Glucose | -275 | - | - | Dardalhon et al, 2012 |
| **$E_{GSH}$ calculated from GSH/GSSG ratio after LC-tandem MS of yeast cells** | | | | | |
| wt | Glucose | -222.78 ± 0.65 | | | Kumar et al, 2011 |
| HGT1[i] | Glucose | -224.02 ± 2.03 | | | Kumar et al, 2011 |
| HGT1 | Glucose + 50 µM GSH | -244.03 ± 2.88 | | | Kumar et al, 2011 |
| HGT1 | Glucose + 100 µM GSH | -249.56 ± 2.88 | | | Kumar et al, 2011 |
| Δ*gsh1*[j] | Glucose | -125.44 ± 0.52 | | | Kumar et al, 2011 |
| Δ*gsh1* | Glucose + 1 µM GSH | -175.27 ± 2.61 | | | Kumar et al, 2011 |
| Δ*gsh1* | Glucose + 100 µM GSH | -202.8 ± 0.51 | | | Kumar et al, 2011 |
| Δ*trr1* | Glucose | -209.69 ± 0.62 | | | Kumar et al, 2011 |

**a)** $E_{GSH}$ determined in *S. cerevisiae* except otherwise indicated, **b)** $E_{GSH}$ were calculated at pH 7.0, **c)** $E_{GSH}$ determined by roGFP1 **d)** $E_{GSH}$ determined by roGFP2, **e)** deletion of thioredoxin reductase, **f)** $E_{GSH}$ [Matrix] was calculated at pH 7.4, **g)** deletion of thioredoxin reductase, **h)** deletion of thioredoxin1 and thioredoxin2, **i)** overexpression of the GSH/GSSG transporter in the plasma membrane, **j)** deletion of ɣ-glutamyl cysteine synthase

## Table S2. Plasmids used in this study

| Plasmid | Characteristics | Primer 5‘-3‘ | Restriction |
|---|---|---|---|
| p416[a)] | TEF promoter, *CEN*-plasmid, *URA3* marker | | |
| p416-Grx1-roGFP2[b)] | Cytosolic form of Grx1-roGFP2 | | |
| p416-$b_2$ | Presequence (1-86) of cytochrome $b_2$ | *F:* TCTAGAATGCTAAAATACAAACCTTTAC TAAAAATC<br>*R:* GGATCCCATATCCAGTTTCGGCTCG | XbaI BamHI |
| p416-$b_2$-Grx1-roGFP2 | Grx1-roGFP2 fused to the presequence (1-86) of cytochrome $b_2$ | *F:* GGATCCGCTCAAGAGTTTGTGAACTGC<br>*R:* AAGCTTTTACTTGTACAGCTCGTCCATG | BamHI HindIII |
| p416-Su9 | Presequence (1-69) of subunit 9 of *Neurospora crassa* ATPase | *F:* TCTAGAATGGCCTCCACTCGTG<br>*R:* GGATCCGGAAGAGTAGGCGCGC | XbaI BamHI |
| p416-Su9-Grx1-roGFP2 | Grx1-roGFP2 fused to the presequence of subunit 9 | *F:* GGATCCGCTCAAGAGTTTGTGAACTGC<br>*R:* AAGCTTTTACTTGTACAGCTCGTCCATG | BamHI HindIII |

a) Mumberg et al, 1995
b) As template p415-Grx1-roGFP2 was used (Morgan et al, 2011)

## Table S3. Strains used in this study

| Strain[a)] | Genotype | Characteristics | Reference |
|---|---|---|---|
| BY4741 | *MAT* a *his3Δ1 leu2Δ0 met15Δ0 ura3Δ0* | | Outten & Culotta, 2004 |
| Δ*glr1* | BY4741 (*MAT*a *his3Δ1 leu2Δ0 met15Δ0 ura3Δ0*) | *GLR1*::*kan*MX4 | Outten & Culotta, 2004 |
| Δ*glr1* + *GLR1* | *MAT*a *his3Δ1 leu2Δ0 met15Δ0 ura3Δ0* | *GLR1* introduced into Δ*glr1* on a plasmid containing *LEU2* | Outten & Culotta, 2004 |
| Δ*glr1* + cyto-*GLR1* | *MAT*a *his3Δ1 leu2Δ0 met15Δ0 ura3Δ0* | Cytosolic *GLR1* introduced into Δ*glr1* on a plasmid containing *LEU2* | Outten & Culotta, 2004 |
| BY4742 | BY4742 (*MATα his3Δ1 leu2Δ0 lys2Δ0 ura3Δ0*) | | Euroscarf |
| Δ*zwf1* | *MATα his3Δ1 leu2Δ0 lys2Δ0 ura3Δ0* | *ZWF1*::*kan*MX4 | Open Biosystems |
| Δ*por1* | *MATα his3Δ1 leu2Δ0 lys2Δ0 ura3Δ0* | *POR1*::*kan*MX4 | Open Biosystems |
| Δ*nde1* | *MATα his3Δ1 leu2Δ0 lys2Δ0 ura3Δ0* | *NDE1*::*kan*MX4 | Open Biosystems |
| Δ*nde2* | *MATα his3Δ1 leu2Δ0 lys2Δ0 ura3Δ0* | *NDE2*::*kan*MX4 | Euroscarf |
| Δ*rip1* | *MATα his3Δ1 leu2Δ0 lys2Δ0 ura3Δ0* | *RIP1*::*kan*MX4 | Euroscarf |
| Δ*cox17* | *MATα his3Δ1 leu2Δ0 lys2Δ0 ura3Δ0* | *COX17*::*kan*MX4 | Euroscarf |
| Δ*ccp1* | *MATα his3Δ1 leu2Δ0 lys2Δ0 ura3Δ0* | *CCP1*::*kan*MX4 | Open Biosystems |
| Δ*sod2* | *MATα his3Δ1 leu2Δ0 lys2Δ0 ura3Δ0* | *SOD2*::*kan*MX4 | Open Biosystems |
| Δ*sod1* | W303 (*MATα ade2-1 ura3-1 his3-11,15 trp1-1 leu2-3,112 can1-100*) | *SOD1*::*HIS3* | Klöppel et al, 2010 |
| W303A GalL-Erv1 | *MATa ade2-1 ura3-1 his3-11,15 trp1-1 leu2-3, 112 can1-100* | *GALL* promoter inserted upstream of *ERV1* | Bien et al, 2010 |
| YPH499 Gal10-Mia40 | *MATa ura3-52 lys2-801_amber ade2-101_ochre trp1-Δ63 his3-Δ200 leu2-Δ1* | *GAL10* promoter inserted upstream of *MIA40* | Terziyska et al, 2005 |
| W303A GalL-Erv1 Δ*glr1* | *MATa ade2-1 ura3-1 his3-11,15 trp1-1 leu2-3, 112 can1-100* | *GLR1*::*kanMX4* | this study |

a) Grx1-roGFP2 sensors were introduced into all yeast strains

## Supplementary Methods

*In vitro fluorescence spectroscopy using purified Grx1-roGFP2 and purified Erv1*

Fluorescence measurements were performed with a spectrofluorometer FP6500 (Jasco) at 25°C with constant stirring in a quartz cuvette (Hellma Analytics, light path 5 mm). Fluorescence was recorded using excitation wavelengths of 405 nm and 488 nm (bandwith ±1.5 nm) and an emission wavelength of 511 nm (bandwith ±1.5). Grx1-roGFP2 and Erv1 were purified as described previously (Bien et al, 2010; Gutscher et al, 2008). Grx1-roGFP2 and Erv1 were diluted in measurement buffer (0.1 M Sorbitol, 0.1 M NaCl, 0.1 M Tris-HCl pH 7.4). 0.5 µM Grx1-roGFP2 were monitored for 10 min and at the indicated time points either buffer, 0.5 µM / 5 µM Erv1 (final concentration), or 50 µM GSSG (final concentration, Sigma-Aldrich) were added.

## Supplementary Figures

**Figure S1. Titration of the Grx1-roGFP2 sensor with diamide and DTT *in vivo*.** Yeast cells expressing cytosolic Grx1-roGFP2 were incubated with the oxidant diamide and the reductant DTT at different concentrations to test for the amounts necessary to achieve full oxidation and full reduction of the sensor, respectively. The concentrations used for further experiments were 20 mM diamide and 100 mM DTT.

**Figure S2. Viability of yeast cells after diamide treatment.** Wild type yeast cells were incubated with 20 mM diamide for the indicated times. Subsequently, cells were washed once in YPD, a tenfold dilution series was plated on YPD plates and growth at 30°C was assessed. Treatment with diamide for the indicated times did not significantly affect subsequent growth on YPD.

**Figure S3. Defining the parameters of the kinetics of recovery of $E_{GSH}$. (A)** Diamide sensitivity of the cytosolic sensor. As Figure 1F, except that different diamide concentrations were used for the oxidative shock. Increasing amounts of diamide resulted in an increasing deviation of the Grx1-roGFP2 redox state from the steady state OxD. Following incubation with diamide concentrations below 20 mM the OxD of the sensor remained below 100%. Upon incubation with 20 and 100 mM diamide the sensor reached 100% oxidation, and recovery started only after an increasingly long lag phase indicating that the glutathione pool had been oxidized beyond the measuring range of the roGFP2 sensor **(B)** Influence of glutathione reductase concentrations on the recovery of the sensor in lysed mitochondria. Mitochondria from strains expressing a matrix targeted variant of Grx1-roGFP2 (see Figure 2A) were isolated. In these isolated mitochondria, the sensor was fully oxidized (= 100 % oxidized Grx1-roGFP2). Mitochondria were lysed and the recovery of the sensor was monitored in the presence of a reducing system composed of NADPH, GSH and varying concentrations of glutathione reductase. The addition of increasing amounts of the enzyme resulted in an increasing recovery rate. The incubation with DTT at the end of the kinetics served as control for fully reduced proteins (= 0 % Grx1-roGFP2). **(C)** Scheme depicting the three parameters to evaluate the recovery kinetics after oxidative shock: (i) lag phase, (ii) recovery rate, and (iii) steady state OxD.

(i) The initial apparent **lag phase** in recovery. Of note, this lag phase does not reflect a delay in the start of the recovery process, but rather represents the time needed for $E_{GSH}$ to drop into the dynamic range of the roGFP2 probe. In other words, the amount of cellular GSSG (*i.e.* $E_{GSH}$) initially remains so high that its reduction to GSH does not (yet) result in sensor reduction. Only when $E_{GSH}$ falls below ~-240 mV Grx1-roGFP2 starts to accompany the recovery process by coupling its own reduction to that of glutathione (Meyer & Dick, 2010). We thus assume that the length of the lag phase correlates with the maximal $E_{GSH}$ reached upon diamide treatment, and thus also represents the sensitivity of the cellular redox environment towards treatment with 20 mM diamide for 5 min.

(ii) The slope of the recovery curve, which reflects the sum of the **rates** of the different reducing systems that contribute to the recovery of the glutathione redox potential back to steady state levels.

(iii) The **steady state** OxD of Grx1-roGFP2, this value indicates the degree of probe oxidation and thus $E_{GSH}$ under unstressed conditions. It reflects the balance of oxidizing and reducing contributions acting on the glutathione pool, and is also dependent on the total glutathione concentration in the respective compartment.

**Figure S4. Steady state redox OxD values and recovery kinetics after oxidative shock in yeast cells grown on glycerol and treated with inhibitors of the respiratory chain. (A)** Steady states of the cytosolic and mitochondrial sensors (Grx1-roGFP2, Su9-Grx1-roGFP2, $b_2$-Grx1-roGFP2) in wild type cells grown on glycerol and treated with KCN (1 mM, 1 hr), antimycin A (AntA; 10 µM, 30 min) and paraquat (5 mM, 30 min). Reported values are the mean of three independent experiments. Error bars are the means ± S.D. Paraquat-treated cells exhibited an increased OxD in the matrix. **(B)** Recovery kinetics after diamide shock on cells expressing Grx1-roGFP2, Su9-Grx1-roGFP2 and $b_2$-Grx1-roGFP2. Wild type cells grown on glycerol were treated with antimycin A (AntA; 10 µM, 30 min) (B), KCN (1 mM, 1 hr) (C), and paraquat (5 mM, 30 min) (D) before diamide incubation and analysis as described in Figure 1F. Reported values are the mean of three independent experiments. Error bars are the means ± S.D. OxD recovery and the lag phase of recovery after diamide treatment were affected in all compartments upon AntA treatment.

**Figure S5. Steady state redox OxD values and recovery kinetics after oxidative shock in yeast cells grown on galactose and treated with inhibitors of the respiratory chain.** This experiment was performed as described in Figure S4 except that cells were grown on galactose. The lag phases of recovery were slightly elongated in all compartments upon Antimycin A and KCN treatment, except for the matrix upon Antimycin A treatment where OxD recovery exhibited an elongated lag phase. The kinetics of recovery upon paraquat treatment were not changed, but recovery took place to the higher OxD[matrix] found at steady state in paraquat-treated cells.

**Figure S6. Steady state redox OxD values and recovery kinetics after oxidative shock in yeast mutants of the respiratory chain grown on galactose.** This experiment was performed as described in Figure S4 except that cells were grown on galactose and analyzed directly. Deletion mutants in *NDE1* (B), *NDE2* (C), *RIP1* (D) and *COX17* (E) were analyzed with the latter two lacking complex III and IV activity, respectively. The IMS sensor in *Δrip1* and *Δcox17* cells recovered to slightly higher steady state OxD values in the IMS after oxidative shock. The matrix sensor in *Δnde2* and *Δcox17* exhibited slightly slower recovery kinetics, and in *Δrip1* the lag phase was slightly elongated.

**Figure S7. Steady state redox OxD values and recovery kinetics after oxidative shock in yeast mutants of the antioxidative defence system.** This experiment was performed as described in Figure S4 except that cells were grown on galactose and analyzed directly. Deletion mutants in *CCP1* (B), *SOD1* (C) and *SOD2* (D) were analyzed. OxD[matrix] recovery after diamide treatment was delayed in the *Δsod2* strain.

**Figure S8. Steady state redox OxD values and recovery kinetics after oxidative shock in yeast cells containing increased levels of enzymes of the oxidative folding machinery. (A)** Protein levels of Mia40 and Erv1 in cells expressing these proteins under the control of a

regulatable promotor, **(B)** Steady states of the cytosolic and mitochondrial sensors (Grx1-roGFP2, Su9-Grx1-roGFP2, $b_2$-Grx1-roGFP2) in wild type cells and cells with increased levels of Mia40 and Erv1. Reported values are the mean of three independent experiments. Error bars are the means ± S.D. Cells containing higher Erv1 levels exhibited an increased OxD[IMS]. **(C, D)** Recovery kinetics after diamide shock on cells expressing Grx1-roGFP2, Su9-Grx1-roGFP2 and $b_2$-Grx1-roGFP2. Cells containing higher levels of Mia40 (C) and Erv1 (D) were analyzed as described in Figure 1F. Reported values are the mean of three independent experiments. Error bars are the means ± S.D. The kinetics of recovery in cells with higher Erv1 levels were not changed, but recovery took place to the higher OxD[IMS] found at steady state in these cells. **(E)** Erv1 does not directly interact with Grx1-roGFP2. Purified Grx1-roGFP2 was reduced with 10 mM DTT. DTT was then removed by gel filtration. 0.5 µM of reduced Grx1-roGFP2 was incubated with either buffer, 50 µM GSSG, 0.5 µM purified Erv1 or 5 µM purified Erv1. Only in the presence of GSSG oxidation of the sensor could be detected. This suggests that the increased OxD[IMS] that is observed upon Erv1 overexpression does not stem from direct oxidation of Grx1-roGFP2 by Erv1.

**Figure S9. Level of mitochondrial proteins in wild type and *Δglr1* cells.** Mitochondria isolated from wild type or *Δglr1* cells were analyzed by Western blot with the indicated antibodies. Mitochondria from both strains contain equal amounts of all indicated proteins.

## Literature for Supplementary Information


Bien M, Longen S, Wagener N, Chwalla I, Herrmann JM, Riemer J (2010) Mitochondrial disulfide bond formation is driven by intersubunit electron transfer in Erv1 and proofread by glutathione. *Mol Cell* **37:** 516-528

Dardalhon M, Kumar C, Iraqui I, Vernis L, Kienda G, Banach-Latapy A, He T, Chanet R, Faye G, Outten CE, Huang M (2012) Redox-sensitive YFP sensors monitor dynamic nuclear and cytosolic glutathione redox changes. *Free Radic Biol Med, in press*

Delic M, Mattanovich D, Gasser B (2010) Monitoring intracellular redox conditions in the endoplasmic reticulum of living yeasts. *FEMS Microbiol Lett* **306:** 61-66

Gutscher M, Pauleau AL, Marty L, Brach T, Wabnitz GH, Samstag Y, Meyer AJ, Dick TP (2008) Real-time imaging of the intracellular glutathione redox potential. *Nat Methods* **5:** 553-559

Hanson GT, Aggeler R, Oglesbee D, Cannon M, Capaldi RA, Tsien RY, Remington SJ (2004) Investigating mitochondrial redox potential with redox-sensitive green fluorescent protein indicators. *J Biol Chem* **279:** 13044-13053

Hu J, Dong L, Outten CE (2008) The redox environment in the mitochondrial intermembrane space is maintained separately from the cytosol and matrix. *J Biol Chem* **283:** 29126-29134

Kloppel C, Michels C, Zimmer J, Herrmann JM, Riemer J (2010) In yeast redistribution of Sod1 to the mitochondrial intermembrane space provides protection against respiration derived oxidative stress. *Biochem Biophys Res Commun* **403:** 114-119

Kumar C, Igbaria A, D'Autreaux B, Planson AG, Junot C, Godat E, Bachhawat AK, Delaunay-Moisan A, Toledano MB (2011) Glutathione revisited: a vital function in iron metabolism and ancillary role in thiol-redox control. *EMBO J* **30:** 2044-2056

Meyer AJ, Dick TP (2010) Fluorescent protein-based redox probes. *Antioxid Redox Signal* **13:** 621-650

Morgan B, Sobotta MC, Dick TP (2011) Measuring E(GSH) and H(2)O(2) with roGFP2-based redox probes. *Free Radic Biol Med* **51:** 1943-1951

Mumberg D, Muller R, Funk M (1995) Yeast vectors for the controlled expression of heterologous proteins in different genetic backgrounds. *Gene* **156:** 119-122

Ostergaard H, Henriksen A, Hansen FG, Winther JR (2001) Shedding light on disulfide bond formation: engineering a redox switch in green fluorescent protein. *EMBO J* **20:** 5853-5862

Ostergaard H, Tachibana C, Winther JR (2004) Monitoring disulfide bond formation in the eukaryotic cytosol. *J Cell Biol* **166:** 337-345

Outten CE, Culotta VC (2004) Alternative start sites in the Saccharomyces cerevisiae GLR1 gene are responsible for mitochondrial and cytosolic isoforms of glutathione reductase. *J Biol Chem* **279:** 7785-7791

Terziyska N, Lutz T, Kozany C, Mokranjac D, Mesecke N, Neupert W, Herrmann JM, Hell K (2005) Mia40, a novel factor for protein import into the intermembrane space of mitochondria is able to bind metal ions. *FEBS Lett* **579:** 179-184

Kojer et al.
Figure S1

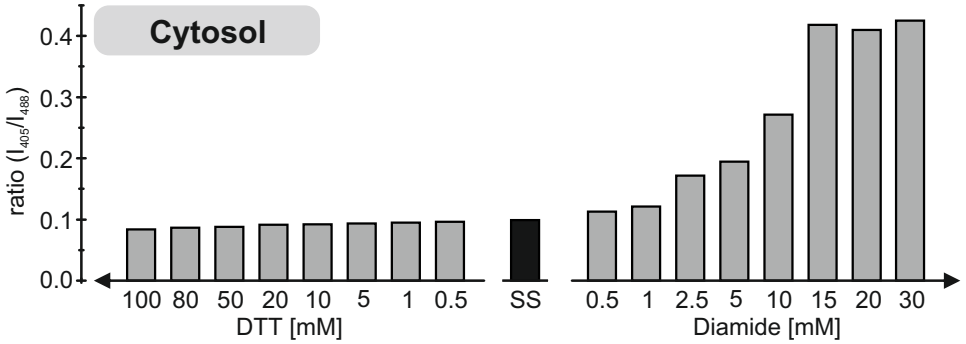

Kojer et al.
Figure S2

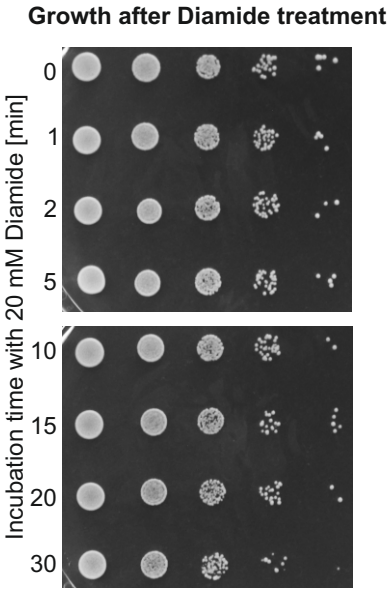

Kojer et al.
Figure S3

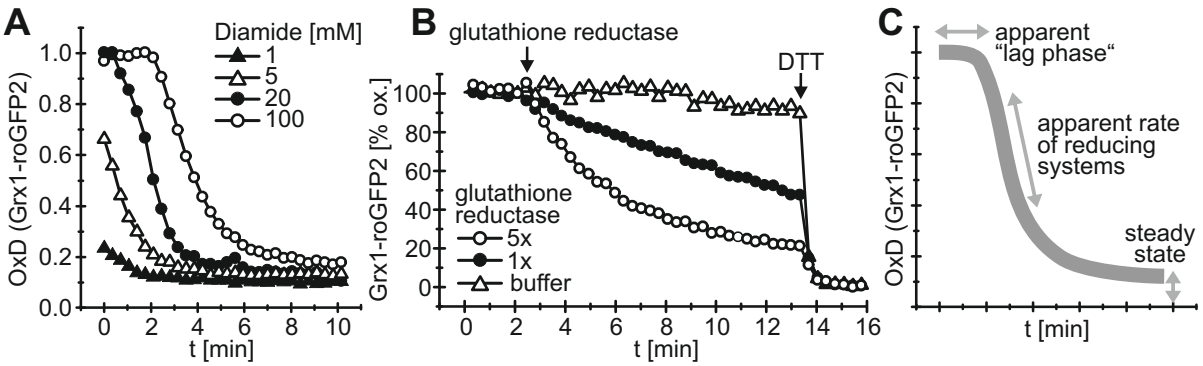

Kojer et al.
Figure S4

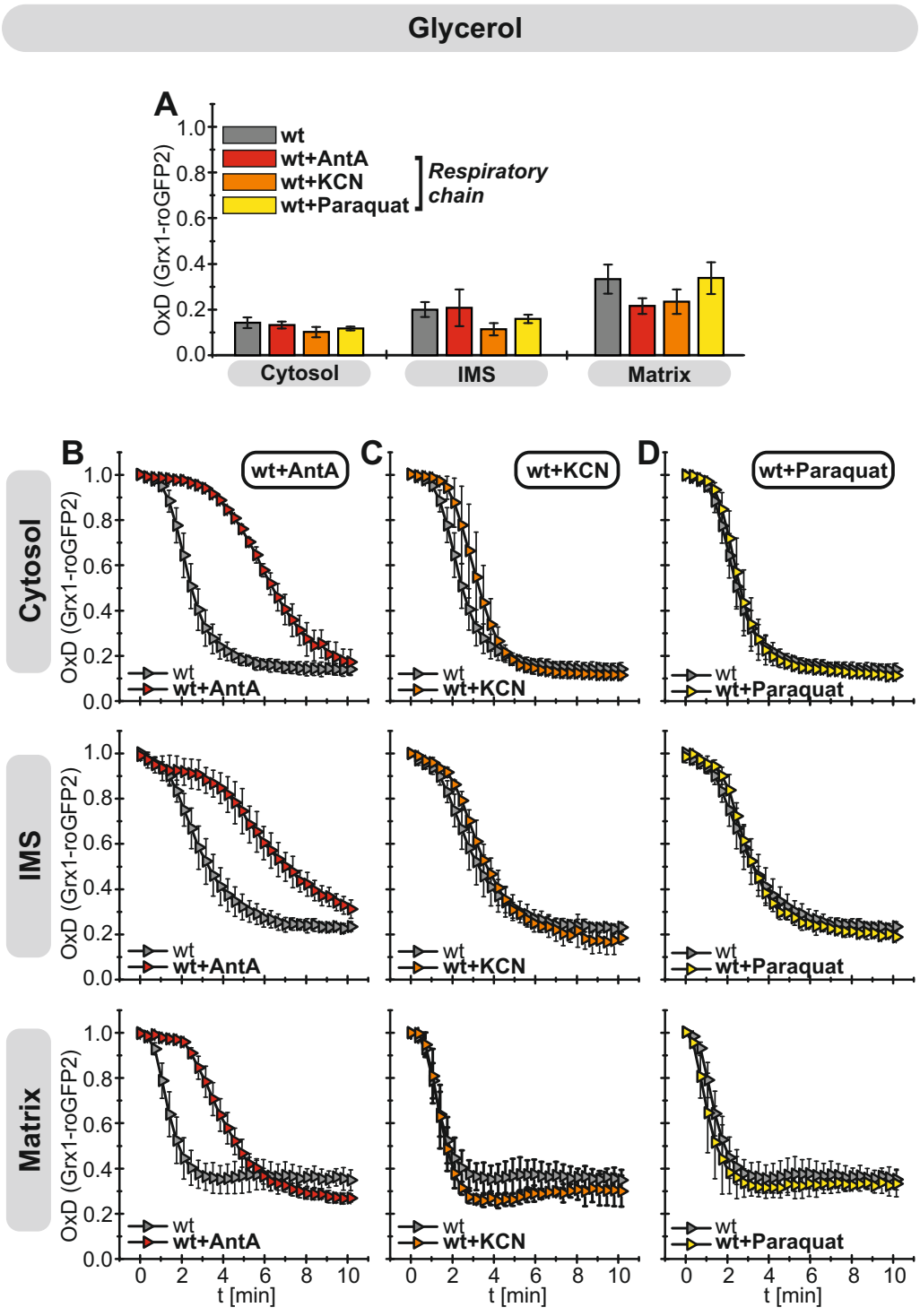

Kojer et al.
Figure S5

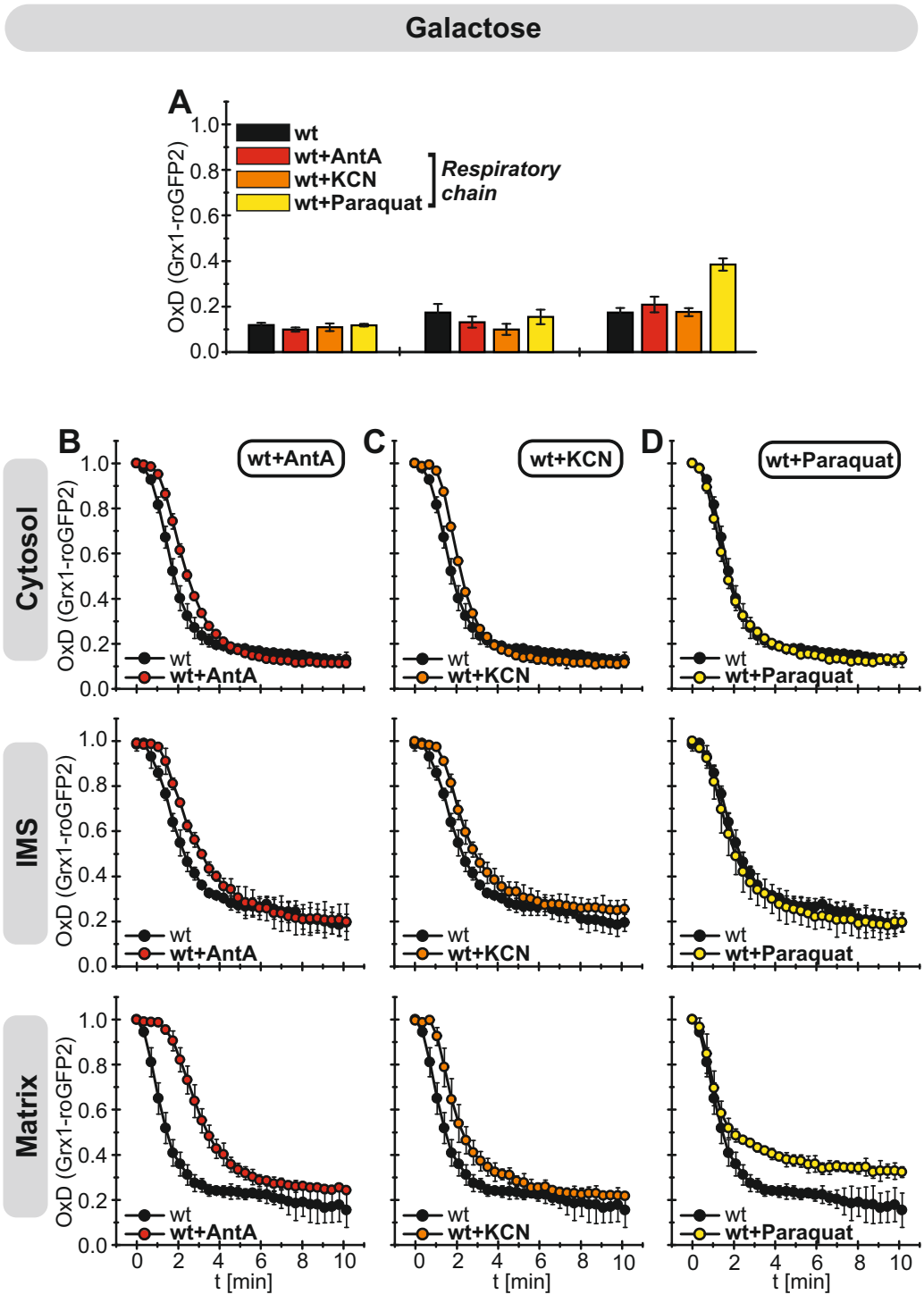

Kojer et al.
Figure S6

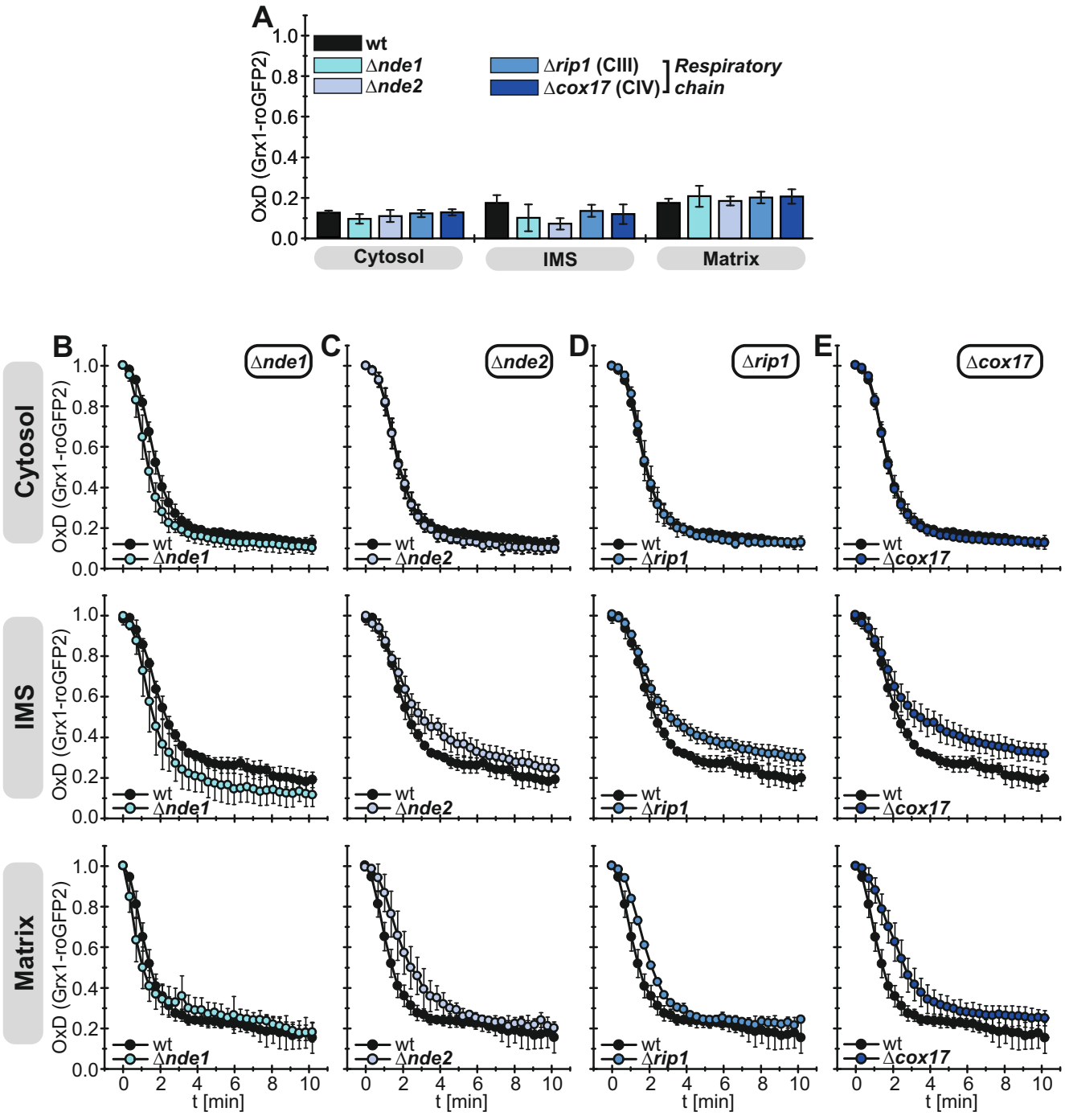

Kojer et al.
Figure S7

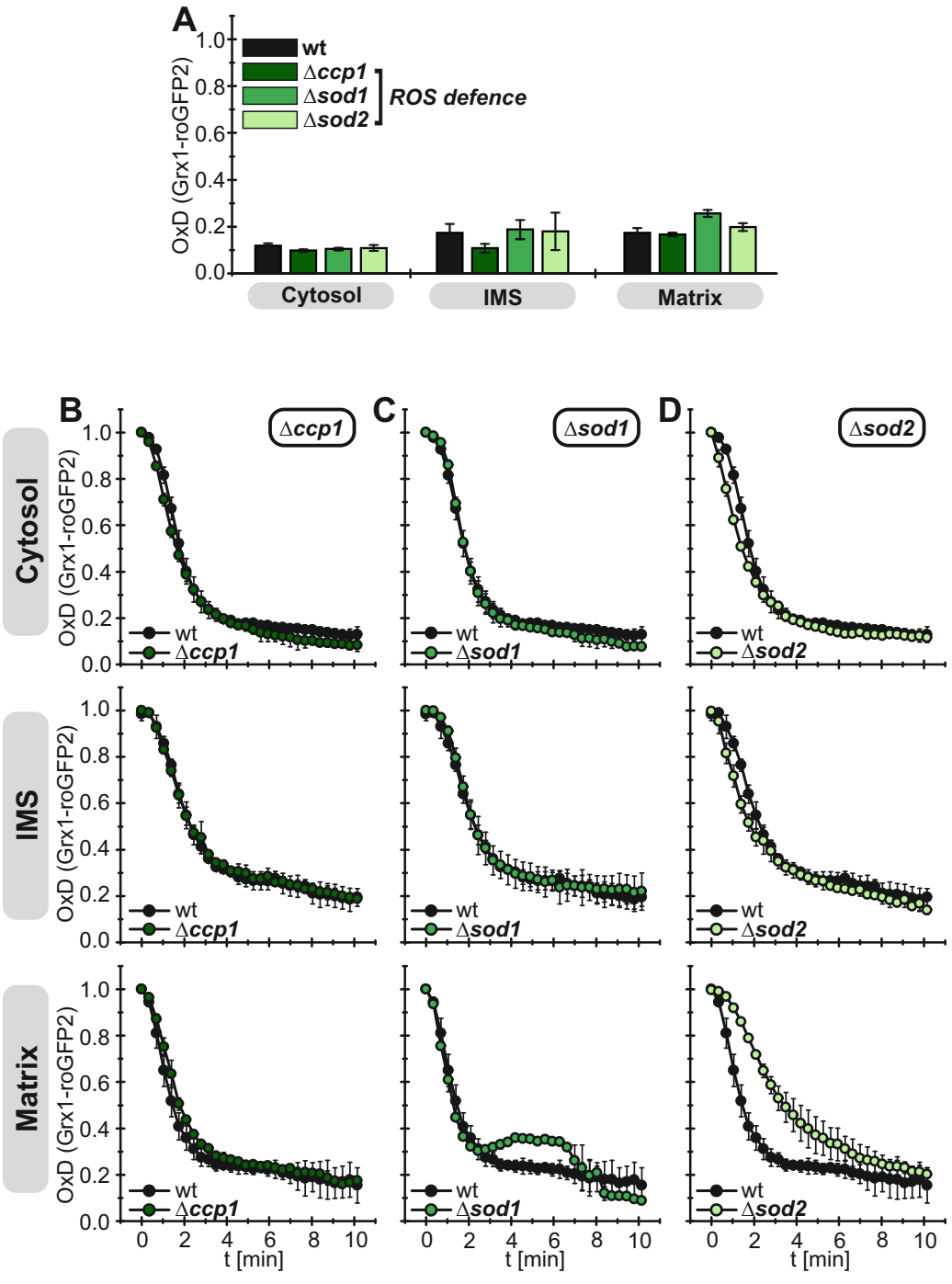

Kojer et al.
Figure S8

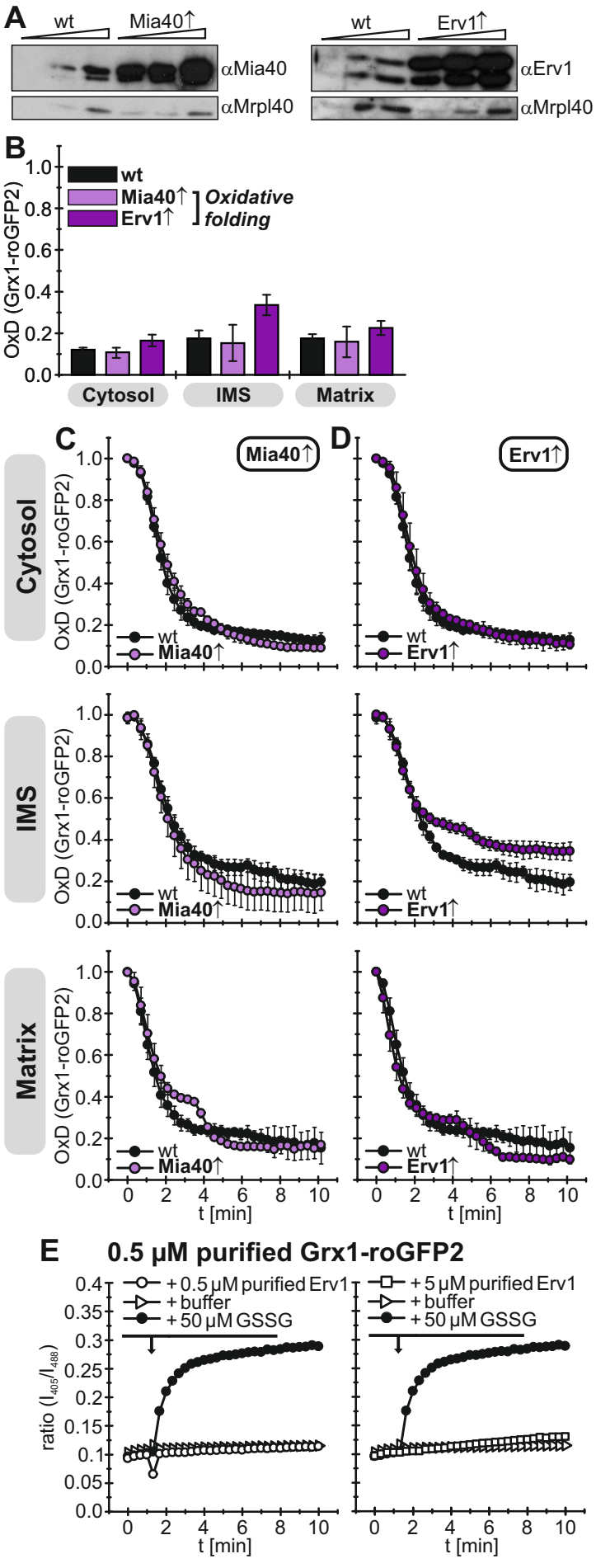

Kojer et al.
Figure S9